

Rapid creation of distant entanglement by multiphoton resonant fluorescence

Guy Z. Cohen* and L. J. Sham

Department of Physics, University of California, San Diego, La Jolla, California 92093-0319

We study a simple, effective and robust method for entangling two separate stationary quantum dot spin qubits with high fidelity using multiphoton Gaussian state. The fluorescence signals from the two dots interfere at a beam splitter. The bosonic nature of photons leads, in analogy with the Hong-Ou-Mandel effect, to selective pairing of photon holes (photon absences in the fluorescent signals). As a result, two odd photon number detections at the outgoing beams herald trion entanglement creation, and subsequent reduction of the trions to the spin ground states leads to spin-spin entanglement. The robustness of the Gaussian states is evidenced by the ability to compensate for photon absorption and noise by a moderate increase in the number of photons at the input. We calculate the entanglement generation rate in the ideal, nonideal and near-ideal detector regimes and find substantial improvement over single-photon schemes in all three regimes. Fast and efficient spin-spin entanglement creation can form the basis for a scalable quantum dot quantum computing network. Our predictions can be tested using current experimental capabilities.

I. INTRODUCTION

Quantum computers have the power to solve some problems much more quickly and efficiently than any classical computer.^{1,2} Quantum communication between two distant elements in the computer or between two quantum computers can be established over a quantum channel and used, e.g., to distribute a key for encrypting data over a classical channel or to establish entanglement, which can then be used for quantum teleportation³ or dense coding.⁴ A leading model for the implementation of these tasks is a quantum network^{5,6} composed of many nodes, each containing one or several quantum bits (qubits), and high fidelity quantum channels connecting these nodes. Preparation, processing and storage of quantum information are performed at the network nodes, which must therefore be stable and in fixed locations (stationary qubits), while quantum communication is attained by photons (flying qubits).

Quantum dot (QD) spin qubits are promising candidates for stationary qubits in scalable quantum networks, as they are compatible with existing semiconductor technology, can be integrated on a chip with photonic crystal cavities,^{7,8} have short optical recombination and photon emission times,^{9,10} can be manipulated by fast single-qubit^{11–14} and two-qubit^{15–18} quantum gates, and can be entangled with adjacent qubits by tunneling interaction¹⁶ or with remote ones via entanglement swapping with photons.^{19–21}

Entanglement of stationary qubits is an essential resource in a quantum network. Inter-qubit entanglement can be applied to increase the quantum capacity of a channel,²² and to implement quantum repeaters²³ for long-distance quantum communication. Entangled qubit pairs can also form the basis for entanglement-assisted quantum error correction (QEC), which has fewer constraints and higher capacity than standard QEC.²⁴ The heralded entanglement of two remote stationary qubits can be achieved by first entangling the

qubits with photons, which interfere on a beam splitter, and then performing a measurement on the photons, with one (type I) or two (type II) single photon detections indicating whether the entanglement creation was successful.^{6,25} Type I heralded entanglement was suggested theoretically^{26,27} and implemented,^{28,29} but suffers from a low success rate due to the requirement of weak qubit excitation and due to high sensitivity to fluctuations in the photonic phase. Type II heralded entanglement schemes,^{30,31} which were also experimentally realized,^{32–34} are exempt from the weak excitation requirement and, through two-photon interference, are more robust to noise than type I schemes. However, both single-photon heralded entanglement types use single-photon states, which are very sensitive to noise, and as a result they currently produce entangled pairs at a slow rate of the order of 0.1 to 10 pairs per minute.^{28,29,32–34} A question is raised whether this performance can be improved by increasing the number of photons at the input.

Several theoretical proposals to improve the entangled pair generation rate by multiphoton light included a system where the matter qubit is placed in a resonant cavity and interacts with coherent state light via coherent Raman scattering,³⁵ whereas the light at the beam splitter output undergoes continuous wave homodyne measurement. The use of multiphoton light, in this case, does not improve the results substantially over single-photon schemes, as the loss of a single photon produces “which path” information which leads to significant decoherence, impairing entanglement creation. Another theoretical work used twin-Fock or NOON states,³⁶ but again produced entanglement creation rates of the same order as single-photon schemes due to sensitivity to single-photon losses. Recently, robust multiphoton entanglement creation using coherent state light was put forward.³⁷ An entanglement creation rate of 1.2×10^7 pairs per minute was calculated for QD spin qubits with this scheme.

Gaussian states form a versatile, robust, powerful, yet simple, continuous variable alternative to qubits in quantum information processing.^{38,39} The single-mode Gaus-

sian state is, in general, squeezed vacuum rotated and displaced in phase space, and thus includes coherent states, squeezed states and thermal states as special cases.³⁸ Multimode Gaussian states, in turn, can exhibit entanglement and be used for quantum cryptography,⁴⁰ quantum teleportation,⁴¹ quantum communication,⁴² quantum computation,⁴³ quantum cloning⁴⁴ and quantum dense coding.⁴⁵ Experimentally, Gaussian states are readily generated with photons^{46,47} and manipulated by many common optical elements, such as beam splitters and quarter-wave plates, which constitute Gaussian operations.³⁸ Gaussian measurements can be performed by homodyne detection.^{48,49}

Among all Gaussian states, the two-mode Gaussian state ($N = 2$), a simple bipartite continuous variable system, attracted much research effort in recent years. The separability criterion was given⁵⁰ as well as a closed expression for the entanglement of formation for symmetric states⁵¹ and the logarithmic negativity entanglement measure for all states.⁵² The purity, von Neumann entropy and mutual information were also found,⁵³ as was the quantum discord,⁵⁴ a measure of the quantumness of correlations for a given state.

We present a simple, effective, robust and scalable multiphoton entanglement generation method driven by two-mode Gaussian state light. Two fluorescence signals interfere at a beam splitter and are then subject to projective photon number measurement. The bosonic statistics of photons gives rise through the *multiphoton Hong-Ou-Mandel effect*, i.e. the Hong-Ou-Mandel effect as applied to photon holes in a multiphoton state, to heralded trion entanglement only upon two odd photon number measurements. Spin entanglement is obtained by reducing the trion states to their corresponding spin states through coherent Rabi rotations in the QDs. In contrast with current single-photon schemes, wherein an excited Λ system must undergo spontaneous emission for entanglement creation,²⁵ the evolution of our 4-level QD spin qubits before the measurement is completely deterministic.

The Gaussian state redundancy provides robustness against noise that is lacking in single-photon or vacuum states. In our system this robustness is manifested in the ability to offset photon absorption, noise and low detection efficiency by a moderate increase in the mean input photon number. We show the entanglement generation rate in our Gaussian state scheme is substantially higher than the ones in single-photon schemes for all three regimes of ideal, nonideal and near-ideal photon number detectors. Even though we have made no direct use of the continuous variable information, the strength of the Gaussian information, we hope that our results from employing the Gaussian states contribute to the viability of this mode of information processing.

The paper is organized as follows. In Sec. II we present the system model and Hamiltonian. We set criteria for the input photon state, find the state satisfying these criteria and solve the Hamiltonian exactly for this state. In

Sec. III we describe the entanglement creation protocol in detail and derive the conditions and probability for heralded entanglement when ideal photon number detectors are employed. In Sec. IV we discuss the effect of decoherence, noise and nonideal detectors on entanglement creation. We arrive at the conditions and probability for heralded entanglement in the nonideal case and analyze the limits and properties of the success probability. In Sec. V we consider the problem of false positive measurements and offer several solutions. Finally, in Sec. VI we discuss the key results and consider directions for future research.

II. SYSTEM MODEL AND HAMILTONIAN

Our system, shown schematically in Fig. 1(a), consists of two four-level, singly charged quantum dots (QDs) in the Faraday geometry^{55,56} in the limit of $\mathbf{B} = 0$ T, a beam splitter and two photomultiplier photon number detectors. We note that the zero magnetic field requirement can be relaxed, so long as the Zeeman-splitting-induced difference in resonance frequency between the two QD level pairs is much lower than the trion state linewidth. The QD energy level diagram is given in Fig. 1(b). The spin state $\pm 1/2$ of each QD functions as a qubit, and the goal is to create entanglement between these two spin qubits. The two levels $|z_{\mp}\rangle$ are degenerate, as are $|t_{\mp}\rangle$. The allowed optical transitions in the first QD are between the $|z_{-}\rangle$ and $|t_{-}\rangle$ levels through σ_{-} polarized light and between the $|z_{+}\rangle$ and the $|t_{+}\rangle$ levels through σ_{+} polarized light, while the cross-spin transitions are forbidden in this geometry. For brevity we take the two QDs to have the same energy levels and denote the QD₂ states by tildes, $|\tilde{z}_{\mp}\rangle, |\tilde{t}_{\mp}\rangle$.

Our protocol for entanglement generation in this system is as follows. The first and second QDs are initially prepared in the $|x_{+}\rangle = (|z_{-}\rangle + |z_{+}\rangle)/\sqrt{2}$ and $|\tilde{x}_{+}\rangle = (|\tilde{z}_{-}\rangle + |\tilde{z}_{+}\rangle)/\sqrt{2}$ states, respectively, by, e.g., a $\pi/2$ laser pulse.⁵⁷ Afterwards, light is shone on each of the QDs and emerges at the beam splitter inputs with a fluorescence signal. The photon states at the beam splitter outputs are detected at the photomultiplier tubes, and the measurement results herald whether distant entanglement between the qubits was achieved.

We choose the composite photon state driving the QDs by specifying a set of conditions which facilitate the entanglement postselection procedure. (1) The state should interact with both level pairs $|z_{\mp}\rangle, |t_{\mp}\rangle$ in each QD, and hence it should be a two-mode state, with polarizations σ_{+} and σ_{-} at the resonance frequency of the levels ω_0 . (2) The state should be a multiphoton Gaussian state, since Gaussian states are expected to be more robust quantum information carriers than single-photon states.³⁸ (3) For simplicity, we follow the common practice^{32,33} in specifying the driving Gaussian state to have the same parameters for the two polarization modes. (4) The Gaussian state should be a pure state.

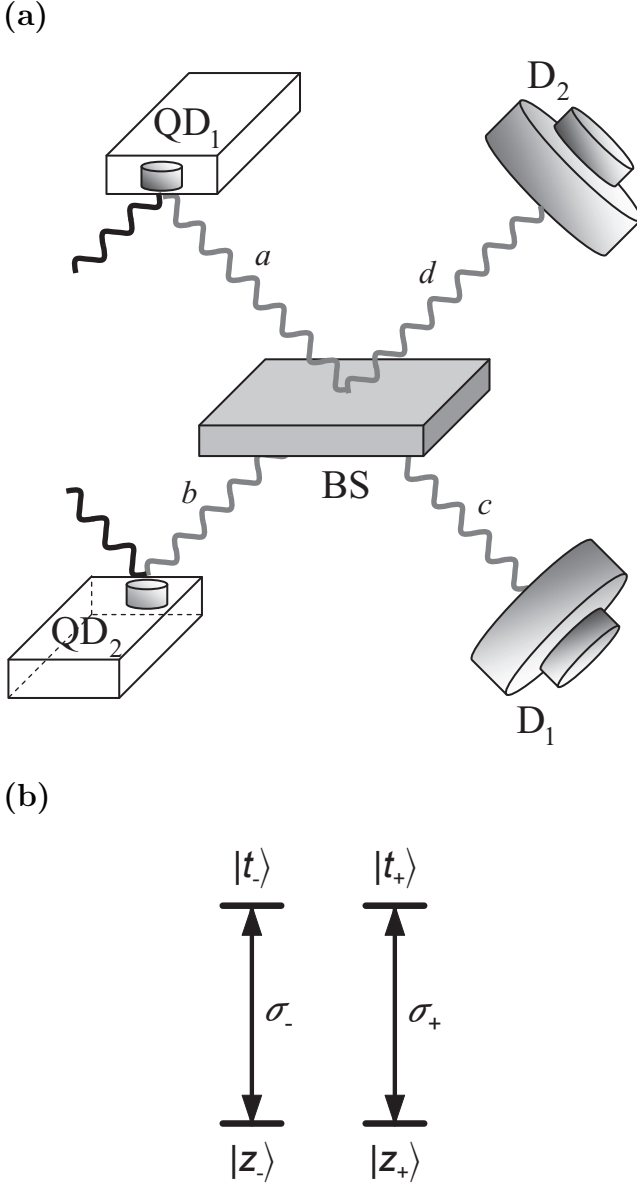


FIG. 1. (a) Schematic of the system for entanglement generation: Two distant quantum dots, QD₁ and QD₂, are driven by coherent light resulting in fluorescence which interferes at a beam splitter, BS. The outputs of the beam splitter are detected by two photomultiplier photon number detectors, D₁ and D₂, which provide postselection of the entangled state. The photon paths are labeled *a*, *b*, *c* and *d*. (b) Energy level diagram for the first dot: The dot is in the Faraday geometry in the limit of $\mathbf{B} = 0$ T, and the allowed transitions are between the $-1/2$ spin state $|z_{-}\rangle$ to the $-3/2$ trion state $|t_{-}\rangle$ and between the $1/2$ spin state $|z_{+}\rangle$ to the $3/2$ trion state $|t_{+}\rangle$ through σ_{\mp} polarized light, respectively. The two states $|z_{\mp}\rangle$ are nearly degenerate, as are $|t_{\mp}\rangle$. The energy level diagram for the second dot is identical except that *z* and *t* have tildes.

The mathematical details of the construction of the Gaussian state with the prerequisites defined above is given in Appendix A. This state is found to be the EPR

state, which in the number state basis reads

$$|\chi(0)\rangle = \sqrt{1-\lambda^2} \sum_{m=0}^{\infty} \lambda^m |m, m\rangle, \quad (1)$$

where $\lambda = \tanh r$, r is the squeezing parameter, and $|m_{-}, m_{+}\rangle$ are the two-polarization mode number basis photon states. The average photon number in the EPR state is the same in both modes,

$$\bar{m} = \frac{\lambda^2}{1-\lambda^2}, \quad (2)$$

which will be used to characterize the input photon state. The variances in the photon number, also identical for both modes, exhibit super-Poissonian statistics, as $\langle(\Delta m)^2\rangle = \bar{m}^2 + \bar{m}$.

The next step is to find the result of the interaction of the designed input photon state with each QD. We model the process by the state evolution of the Jaynes-Cummings Hamiltonian⁵⁸

$$H = H_0 + H_1, \quad (3)$$

$$H_0 = \omega_0 \sum_i a_i^\dagger a_i + \frac{\omega_0}{2} \sum_i \left(|t_i\rangle\langle t_i| - |z_i\rangle\langle z_i| \right), \quad (4)$$

$$H_1 = g \sum_i \left(a_i^\dagger |z_i\rangle\langle t_i| + \text{h.c.} \right), \quad (5)$$

where \hbar is taken as unity, g is the coupling constant, and a_i and a_i^\dagger are the annihilation and creation operators for a σ_i polarized photon with the resonance frequency ω_0 . This evolution idealizes the scattering process of the light against the quantum dot and the host matrix by assuming it is entirely reflected by the solid system. This mirror can be approximated by the reflection of the quantum dot grown on a substrate on top of a metal gate. We attempt here only a conceptual formulation and recognize the limitation of this aspect of the estimate of the entanglement efficiency as lacking in accuracy for an experimental design. The idealization neglects the photon loss in the actual physical processes. Possible remedies include wave guides as conduit of photon states and embedding each QD in a Fabry-Pérot microcavity tuned to have modes in resonance with the QD transitions [Fig. 1(b)]. We provide in the conclusions section an estimate of the errors if the latter method is employed.

The Hamiltonian in the interaction representation is the time independent H_1 because of the resonance condition. The state is governed by the Schrödinger equation

$$i \frac{\partial}{\partial t} |\psi(t)\rangle = H_1 |\psi(t)\rangle \quad (6)$$

with the initial condition being the product of the QD initial condition and the photon state in Eq. (1),

$$|\psi(0)\rangle = |x_{+}\rangle |\chi(0)\rangle. \quad (7)$$

The exact solution at time t of Eq. (6) with the Hamiltonian (5) is

$$|\psi_a(t)\rangle = |x_{+}\rangle |\chi(t)\rangle + |t_{-}\rangle |\chi_{-}(t)\rangle + |t_{+}\rangle |\chi_{+}(t)\rangle, \quad (8)$$

where the subscript *a* denotes the photon path in Fig. 1, and the photon conditional states are

$$|\chi(t)\rangle = \sqrt{1-\lambda^2} \sum_{m=0}^{\infty} \lambda^m \cos(g\sqrt{m}t) |m, m\rangle, \quad (9)$$

$$|\chi_{-}(t)\rangle = -i\sqrt{\frac{1-\lambda^2}{2}} \sum_{m=0}^{\infty} \lambda^m \sin(g\sqrt{m}t) |m-1, m\rangle, \quad (10)$$

$$|\chi_{+}(t)\rangle = -i\sqrt{\frac{1-\lambda^2}{2}} \sum_{m=0}^{\infty} \lambda^m \sin(g\sqrt{m}t) |m, m-1\rangle. \quad (11)$$

We see the interaction results in photon and qubit states entanglement, which will be useful for inter-qubit entanglement creation. The beam splitter input state is thus $|\psi_a(t)\rangle|\psi_b(t)\rangle$, with $|\psi_a(t)\rangle$ given in Eq. (8) and $|\psi_b(t)\rangle$, the state corresponding to the b photon path and the second QD, obtained from the same equation by writing it in terms of $|\tilde{x}_{+}\rangle$ and $|\tilde{t}_{\pm}\rangle$.

III. ENTANGLEMENT GENERATION

We detail the entanglement process. The input states to the beam splitter from the two QD's driven by coherent light interfere at the beam splitter. The total number of photons at each output is measured by a detector [see Fig. 1(a)], and an entangled state is then selected after obtaining the appropriate pair of photon numbers in the two paths. Let the input composite photon basis state be $|m_{-}, m_{+}; \tilde{m}_{-}, \tilde{m}_{+}\rangle_{a,b}$, which corresponds to m_{-} and m_{+} photons of respective polarizations σ_{\mp} along path a from QD₁, and $\tilde{m}_{-}, \tilde{m}_{+}$ photons along path b from QD₂. The output state is a linear combination of the output composite basis states $|m'_{-}, m'_{+}; \tilde{m}'_{-}, \tilde{m}'_{+}\rangle_{c,d}$, along paths c, d , defined analogously to the input basis states. The two basis sets are related by the unitary transformation of the single photon by the beam splitter,

$$\begin{aligned} c_i &= \frac{1}{\sqrt{2}}(a_i + b_i), \\ d_i &= \frac{1}{\sqrt{2}}(b_i - a_i), \end{aligned} \quad (12)$$

where a_i, b_i , are the annihilation operators of incoming photons of polarization $i = \mp$ along paths a, b , respectively, and, similarly, c_i, d_i denote the outgoing photons.

The detection process can be described by projection operators,¹ each of which corresponds to a measurement result. Since the photodetection is insensitive to polarization, the projector for a measurement of n_1 and n_2 photons in the first and second detectors, respectively, is

$$P_{n_1, n_2} = \sum_{k=0}^{n_1} \sum_{l=0}^{n_2} |k, n_1 - k; l, n_2 - l\rangle \langle k, n_1 - k; l, n_2 - l|. \quad (13)$$

As these projectors are orthonormal, i.e. $P_{n_1, n_2} P_{n'_1, n'_2} = \delta_{n_1, n'_1} \delta_{n_2, n'_2} P_{n_1, n_2}$, the measurement is a von Neumann measurement, and the state after the measurement is

$$|\psi_{n_1, n_2}\rangle = P_{n_1, n_2} |\psi(t)\rangle, \quad (14)$$

where $|\psi(t)\rangle$ is the state of the system after the beam splitter and before the measurement. The probability for this measurement is

$$\text{Prob}_{n_1, n_2}(\overline{m}, t) = \langle \psi(t) | P_{n_1, n_2} | \psi(t) \rangle. \quad (15)$$

The measurement probability Prob_{n_1, n_2} has the same form in the Schrödinger picture as in the interaction picture, since the transition to the former in Eq. (15), which includes insertion of $\exp(iH_0t)$ and $\exp(-iH_0t)$ operators, leads to the same expression. Thus Prob_{n_1, n_2} , calculated in the interaction picture, corresponds to the measurement probability of n_1 and n_2 photons at time t .

Consider first the case when n_1 is even and n_2 is odd or vice versa. The state after the measurement is

$$|\psi_{n_1, n_2}\rangle = P_{n_1, n_2} U_{BS} [|\psi_a(t)\rangle |\psi_b(t)\rangle], \quad (16)$$

where U_{BS} is the beam splitter transformation operator, and $|\psi_{a,b}(t)\rangle$ are given in Eq. (8). The P_{n_1, n_2} and U_{BS} operators act only on the 9 conditional photon states in $|\psi_a(t)\rangle |\psi_b(t)\rangle$, and as U_{BS} conserves the total number of photons, only the terms in $|\psi_a(t)\rangle |\psi_b(t)\rangle$ with an odd number of photons contribute. Of these terms $|\chi_{\mp}\rangle |\chi_{\mp}\rangle$ differs from $|\chi_{\mp}\rangle |\chi_{\mp}\rangle$ by $m_{\mp} \leftrightarrow \tilde{m}_{\mp}$ in each composite photon state $|m_{-}, m_{+}; \tilde{m}_{-}, \tilde{m}_{+}\rangle_{a,b}$ in it. This transposition is the same as $a_i \leftrightarrow b_i$, which after the beam splitter transformation (12), is equivalent to $d_i \rightarrow -d_i$ and gives a $(-1)^{n_2}$ overall factor. The state after the measurement is thus

$$|\psi_{n_1, n_2}\rangle = P_{n_1, n_2} U_{BS} \{ |A_{-}\rangle |\chi_{-}\rangle |\chi_{-}\rangle + |A_{+}\rangle |\chi_{-}\rangle |\chi_{+}\rangle \}, \quad (17)$$

where $|A_{\mp}\rangle = |x_{+}\rangle |\tilde{t}_{\mp}\rangle + (-1)^{n_2} |t_{\mp}\rangle |\tilde{x}_{+}\rangle$.

The terms $P_{n_1, n_2} U_{BS} (|\chi_{\mp}\rangle |\chi_{\mp}\rangle)$ in Eq. (17) have the same norm and are orthogonal, since $|\chi_{\mp}\rangle |\chi_{\mp}\rangle$ differ only by an exchange of polarizations and are orthogonal, a property preserved by P_{n_1, n_2} and U_{BS} . As $|A_{-}\rangle$ and $|A_{+}\rangle$ have the same norm and are orthogonal, the state following a $-$ or $+$ measurement at one QD carries no preference for $-$ or $+$ at the other QD, and $|\psi_{n_1, n_2}\rangle$ has no spin entanglement.

Next, consider the cases where both n_1 and n_2 are odd or both n_1 and n_2 are even. The state after the measurement is again given by Eq. (16), but now the contributing terms have an even total photon number. Of these terms $|\chi_{-}\rangle |\chi_{+}\rangle$ differs from $|\chi_{+}\rangle |\chi_{-}\rangle$ by $a_i \leftrightarrow b_i$, which after the beam splitter transformation (12), is equivalent to $d_i \rightarrow -d_i$ and gives an overall sign of \mp in the odd-odd and even-even cases, respectively. The state after the measurement reads

$$|\psi_{n_1, n_2}\rangle = P_{n_1, n_2} U_{BS} \{ |B_0\rangle |\chi_{+}\rangle |\chi_{+}\rangle + |B_{\downarrow}\rangle |\chi_{-}\rangle |\chi_{-}\rangle + |B_{\uparrow}\rangle |\chi_{+}\rangle |\chi_{+}\rangle + |B_{\mp}\rangle |\chi_{-}\rangle |\chi_{+}\rangle \}, \quad (18)$$

where $|B_0\rangle = |x_{+}\rangle |\tilde{x}_{+}\rangle$, $|B_{\downarrow}\rangle = |t_{-}\rangle |\tilde{t}_{-}\rangle$, $|B_{\uparrow}\rangle = |t_{+}\rangle |\tilde{t}_{+}\rangle$, and $|B_{\mp}\rangle = (|t_{-}\rangle |\tilde{t}_{+}\rangle \mp |t_{+}\rangle |\tilde{t}_{-}\rangle)$ are the QD conditional states in the odd-odd and even-even cases, respectively. The photon states multiplying each of $|B_0\rangle$, $|B_{\downarrow}\rangle$ and $|B_{\uparrow}\rangle$ are invariant under $a_i \leftrightarrow b_i$, which corresponds to

$d_i \rightarrow -d_i$ after the beam splitter transformation. They therefore contribute only to the even-even case, and the state in the odd-odd case is $|B_-\rangle P_{n_1, n_2} U_{BS}(|\chi_-\rangle|\chi_+\rangle)$, separable to a photon state and qubit state of $|\Psi_-\rangle = \frac{1}{\sqrt{2}}(|t_-\rangle|\tilde{t}_+\rangle - |t_+\rangle|\tilde{t}_-\rangle)$, Bell's fourth state, which is maximally entangled. By the selection rules in Fig. 1(b), each trion state decays spontaneously to the corresponding spin state with a random phase. To preserve the entanglement and avoid the delay, the trion states should instead be reduced to the spin states by applying on each QD a pair of phase-locked π -pulses with polarizations σ_\mp .

Having shown that an odd-odd measurement heralds QD spin entanglement, we wish to investigate the even-even case. The QD density matrix, found from Eq. (18) by tracing over the photons in $|\psi_{n_1, n_2}\rangle\langle\psi_{n_1, n_2}|$, is in this case, up to normalization,

$$\rho = q_0|B_0\rangle\langle B_0| + q_\downarrow(|B_\downarrow\rangle\langle B_\downarrow| + |B_\uparrow\rangle\langle B_\uparrow|) + q_+|B_+\rangle\langle B_+|, \quad (19)$$

where the conservation of total photon number in each polarization was used to show that the photon states associated with $|B_0\rangle$, $|B_\downarrow\rangle$, $|B_\uparrow\rangle$, and $|B_+\rangle$ in Eq. (18) do not lead to cross terms in the QD density matrix. The terms $|B_\downarrow\rangle\langle B_\downarrow|$ and $|B_\uparrow\rangle\langle B_\uparrow|$ have the same coefficient in Eq. (19), since the photon states associated with $|B_\downarrow\rangle$ and $|B_\uparrow\rangle$ in Eq. (18) are identical apart from an exchange of the polarizations. The QD density matrix in Eq. (19) is a mixture of the density matrix $q_0|B_0\rangle\langle B_0|$, which is separable by the form of $|B_0\rangle$, and the density matrix given by the rest of Eq. (19). The last density matrix has $q_\downarrow \geq q_+$, as shown in Appendix B, and thus has zero concurrence.⁵⁹ We conclude we have no spin entanglement in the even-even case, as the density matrix in Eq. (19) is separable, being a mixture of two separable density matrices.¹

The association of spin entanglement with odd-odd measurements can also be seen to emerge from the bosonic nature of photons. The interaction with the QDs results in coupling photon hole states to $|t_-\rangle$ and $|t_+\rangle$ in Eq. (8). The part of $|\psi_a(t)\rangle|\psi_b(t)\rangle$ with no photon holes has an even total photon number and a photon state symmetric under $a_i \leftrightarrow b_i$ and hence must produce only even-even measurements. The parts with a single photon hole have an odd total photon number and contribute to odd-even or even-odd measurements. The parts involving two photon holes with the same polarization are associated with $|t_\mp\rangle|\tilde{t}_\mp\rangle$. For these parts, the photon holes interfere, owing to their bosonic statistics, à la the Hong-Ou-Mandel (HOM) effect⁶⁰ to give a pair of holes at either one of the detectors, keeping the even-even measurement. This effect may be termed the *multiphoton HOM effect*, as photon holes exist in a background multiphoton state. The parts involving two photon holes with different polarizations are associated with $|t_\mp\rangle|\tilde{t}_\pm\rangle$. The photon holes evolve independently then and can either end up at the same detector or separate to give an odd-odd measurement. The photon state contributing to this measurement is the one antisymmetric under $a_i \leftrightarrow b_i$. Since the

associated qubit state is $|\Psi_-\rangle$, an odd-odd measurement heralds spin entanglement.

Having dealt with the states after the measurements, we now analyze the probability to obtain a measurement result, Prob_{n_1, n_2} in Eq. (15). First, since the beam splitter inputs are identical,

$$\text{Prob}_{n_1, n_2}(\bar{m}, t) = \text{Prob}_{n_2, n_1}(\bar{m}, t). \quad (20)$$

We are only interested in the odd-odd case for Prob_{n_1, n_2} , as this is when entanglement is generated. By Eq. (15) $\text{Prob}_{n_1, n_2} = |P_{n_1, n_2}|\psi(t)\rangle|^2$. The discussion following Eq. (18) points to the term multiplying $|B_-\rangle$ as the only one remaining in $|\psi_{n_1, n_2}\rangle$ in the odd-odd case, whereupon by Eq. (18)

$$\text{Prob}_{n_1, n_2} = |P_{n_1, n_2} U_{BS}|\chi_-\rangle|\chi_+\rangle|^2. \quad (21)$$

Plugging in P_{n_1, n_2} from Eq. (13) in Eq. (21), using total photon number conservation, and the beam splitter matrix elements being real, we obtain

$$\text{Prob}_{n_1, n_2} = \frac{1}{2}(1 - \lambda^2)^2 \lambda^{2(n_3+1)} \sum_{k=0}^{n_1} \sum_{l=0}^{n_2} \times \left[\sum_{m=0}^{n_3} \sin(g\sqrt{m}t) \sin(g\sqrt{m'}t) F_{klmm'} \right]^2, \quad (22)$$

where $n_3 = (n_1 + n_2)/2$, $m' = n_3 + 1 - m$, and $F_{klmm'} = \langle k, n_1 - k; l, n_2 - l | U_{BS} | m - 1, m; m', m' - 1 \rangle$. The measurement probability in Eq. (22) is seen to be separable to an \bar{m} -dependent part and a time dependent part. With the aid of Eq. (2) we have $\text{Prob}_{n_1, n_2}(\bar{m}, t) = f_{n_1, n_2}(\bar{m}) g_{n_1, n_2}(t)$ with

$$f_{n_1, n_2}(\bar{m}) = \frac{1}{(\bar{m} + 1)^2} \left(\frac{\bar{m}}{\bar{m} + 1} \right)^{n_3+1} \quad (23)$$

and

$$g_{n_1, n_2}(t) = \frac{1}{2} \sum_{k=0}^{n_1} \sum_{l=0}^{n_2} \times \left[\sum_{m=0}^{n_3} \sin(g\sqrt{m}t) \sin(g\sqrt{m'}t) F_{klmm'} \right]^2. \quad (24)$$

The two time scales in the Hamiltonian (3) are the reciprocals of the light frequency ω_0 and the coupling constant g . If the time interval between detections is much higher than $\frac{2\pi}{g}$, which is typically^{56,61} of the order of 1ns, then for $g_{n_1, n_2}(t)$ in Eq. (24) only the time average is of practical interest. Let us denote this average as C_{n_1, n_2} and the time-averaged probability of measurement as

$$\overline{\text{Prob}}_{n_1, n_2}(\bar{m}) = \frac{C_{n_1, n_2}}{(\bar{m} + 1)^2} \left(\frac{\bar{m}}{\bar{m} + 1} \right)^{n_3+1}, \quad (25)$$

where Eq. (23) was used. The form of C_{n_1, n_2} is found in Appendix C and used to plot $\overline{\text{Prob}}_{n_1, n_2}(\bar{m})$ for several values of n_1 and n_2 in Fig. 2. The maximum of this function occurs at $\bar{m} = (n_3 + 1)/2$.

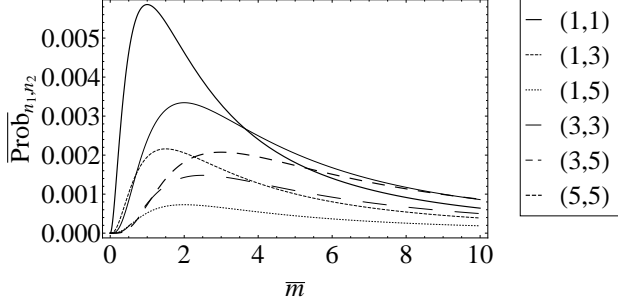


FIG. 2. Time-averaged probability for measuring (n_1, n_2) in detectors D_1 and D_2 , respectively, as a function of the average input photon number \bar{m} for selected odd-odd pairs of (n_1, n_2) .

The probability of both detectors measuring an odd number of photons is

$$\text{ProbSucc}(\bar{m}, \eta = 1) = \sum_{n_1=1,3,\dots}^{\infty} \sum_{n_2=1,3,\dots}^{\infty} \overline{\text{Prob}}_{n_1, n_2}(\bar{m}), \quad (26)$$

Substitution of Eq. (25) in Eq. (26) leads to

$$\text{ProbSucc}(\bar{m}, \eta = 1) = \frac{\sum_{n_3=1}^{\infty} D_{n_3} \left(\frac{\bar{m}}{\bar{m}+1} \right)^{n_3+1}}{(\bar{m}+1)^2}, \quad (27)$$

where

$$D_{n_3} = \sum_{n_1=1,3,\dots}^{n_3} C_{n_1, 2n_3-n_1} = \frac{n_3}{16} + \frac{1 - (-1)^{n_3}}{64}, \quad (28)$$

the sum over n_1 being evaluated using Eq. (C5). Equation (27) reduces to the simple form,

$$\text{ProbSucc}(\bar{m}, \eta = 1) = \frac{1}{32} \frac{4\bar{m} + 3}{2\bar{m} + 1} \left(\frac{\bar{m}}{\bar{m} + 1} \right)^2 \quad (29)$$

plotted in Fig. 3. The asymptotic success probability at $\bar{m} \rightarrow \infty$ is seen by Eq. (29) to be $1/16$. Since the success probability is monotonously increasing, we define the characteristic value of \bar{m} needed to obtain entanglement, $\bar{m}_{1/2}$, as the one giving half this probability. This value for ideal detectors is, by Eq. (29), $\bar{m}_{1/2} \approx 2.08$.

IV. IMPACT OF NOISE

We will now discuss possible sources of noise which affect the entanglement generation. The important factor is the effective detector efficiency η , which is the product of optical transmission factors, detector light collection solid angle ratio and detector quantum efficiency. The noise from imperfect generation of the EPR state is negligible, as this state can be prepared with high fidelity.^{62,63}

The noise from imperfect beam splitter and photon loss in the medium can be dealt with by introducing a constant multiplicative factor at the effective detector efficiency η .^{32,63} In addition, current typical detector dark count rates¹⁹ of ~ 100 Hz are much lower than the entanglement creation rate, and the spin qubit decoherence time of $\sim 1 \mu\text{s}$, attainable by nuclear spin quieting techniques,^{64,65} is much larger than the time needed to generate entanglement following qubit state preparation.

The probability to measure m photons using a detector of efficiency η is given by the quantum theory of photodetection⁶¹ as

$$\bar{P}_m = \sum_{n=m}^{\infty} \bar{P}_n \binom{n}{m} \eta^m (1-\eta)^{n-m}, \quad (30)$$

where \bar{P}_n is the probability for n photons at the detector input state. For a number state of q photons, $\bar{P}_n = \delta_{q,n}$, and the probability to measure zero photons is, by Eq. (30), $\bar{P}_0 = (1-\eta)^q$. This is the important probability for us, since measuring zero photons in either one of the detectors indicates that either the number of photons is zero, for which we get no entanglement, or that the detector did not interact with the light at all.

With nonideal detectors^{32,33} $\eta \ll 1$, and discerning the odd-odd measurement results from the rest is not realistic. We therefore consider coincident clicks in both detectors as a positive result with the understanding that some false positive readings will occur. With this understanding, the success probability for nonideal detectors is

$$\text{ProbSucc}(\bar{m}, \eta) = \sum_{n_1} \sum_{n_2} \overline{\text{Prob}}_{n_1, n_2}(\bar{m}) (1 - (1-\eta)^{n_1}) (1 - (1-\eta)^{n_2}), \quad (31)$$

where the sum over n_1 and n_2 is, as usual, only over the odd integers, and $\overline{\text{Prob}}_{n_1, n_2}(\bar{m})$ is given in Eq. (25). Equation (31) reduces to Eq. (26) in the ideal detector limit of $\eta = 1$. For other values of η Eq. (31) is evaluated in Appendix D and plotted in Fig. 3. We find the asymptotic value of the success probability is still $1/16$ as in the ideal case, but higher values of \bar{m} are needed to obtain a given success probability.

Consider now the behavior of the $\text{ProbSucc}(\bar{m}, \eta)$ function at various limits. First, at $\bar{m} \ll 1$, we see from Eq. (25) that the dominant term in Eq. (31) is the one with $n_1 = n_2 = 1$. In this limit we thus have

$$\text{ProbSucc}(\bar{m}, \eta) \approx \frac{3}{32} (\bar{m}\eta)^2. \quad (32)$$

The asymptotic behavior at $\bar{m} \rightarrow \infty$ can be found by the approximations in Appendix D, which, as noted there, are exact at this limit. We find

$$\text{ProbSucc}(\bar{m}, \eta) \approx \frac{1}{16} - \frac{1}{\bar{m}} \left[\frac{7\eta^2 - 6\eta - 8}{4\eta(\eta - 2)} \right]. \quad (33)$$

When $\eta \ll 1$ Eq. (33) reduces to

$$\text{ProbSucc}(\bar{m}, \eta) \approx \frac{1}{16} - \frac{1}{\bar{m}\eta}, \quad (34)$$

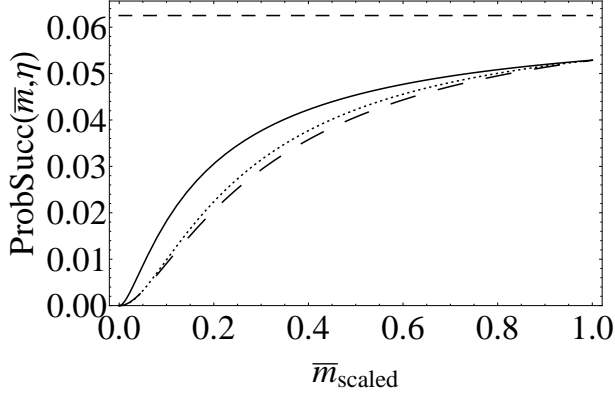


FIG. 3. Success probability of entanglement creation vs the scaled average number of photons at the input EPR state when the effective detector efficiency is $\eta = 1, 0.1, 0.01$ and $\bar{m}_{\text{scaled}} = \bar{m}/10, \bar{m}/33.3, \bar{m}/251$, respectively (solid, dotted, large dashes). The average number of photons at the input EPR state is \bar{m} , and the scaling was chosen so as to make the value at $\bar{m}_{\text{scaled}} = 1$ identical for the three values of η . The line for $\eta = 0.001$ with the scaling of $\bar{m}_{\text{scaled}} = \bar{m}/2440$ was not plotted as it coincided with the line for $\eta = 0.01$ to within 0.5%. The reason for the coincidence is the scaling law, which applies at $\eta \ll 1$ and gives the success probability $\text{ProbSucc}(\bar{m}, \eta) = \text{ProbSucc}(\lambda \bar{m}, \lambda^{-1} \eta)$, where λ is the scaling constant. The horizontal dashed curve shows the asymptotic value of $1/16$ for the probability at $\bar{m} \rightarrow \infty$, which is the same for all values of η .

which is a function of $\bar{m}\eta$, as was the case in Eq. (32) for $\bar{m} \ll 1$. By the approximations in Appendix D we find this dependence holds for all values of \bar{m} when $\eta \ll 1$, and in particular for $\bar{m}_{1/2}$, defined above by $\text{ProbSucc}(\bar{m}_{1/2}, \eta) = 1/32$, as shown in Fig. 4. Consequently, the success probability satisfies the *scaling law*⁶⁶

$$\text{ProbSucc}(\bar{m}, \eta) = \text{ProbSucc}(\lambda \bar{m}, \lambda^{-1} \eta), \quad (35)$$

where λ is a constant. This scaling law means that increasing the average EPR state photon number by a factor of λ is equivalent to improving the detector efficiency by the same factor. The dependence of the $\text{ProbSucc}(\bar{m}, \eta)$ function on a single variable $\bar{m}\eta$ enables us to calculate the value of the function for arbitrary values of η or \bar{m} , so long as scaling applies, by its values for a single value of \bar{m} or η . This property is called *data collapse*.⁶⁶

V. FALSE POSITIVE READINGS

The entanglement creation success probability was seen to reach the same asymptotic value of $1/16$ when the mean input photon number \bar{m} is large enough to compensate for the low detector efficiency. However, this success probability is merely the probability of true posi-

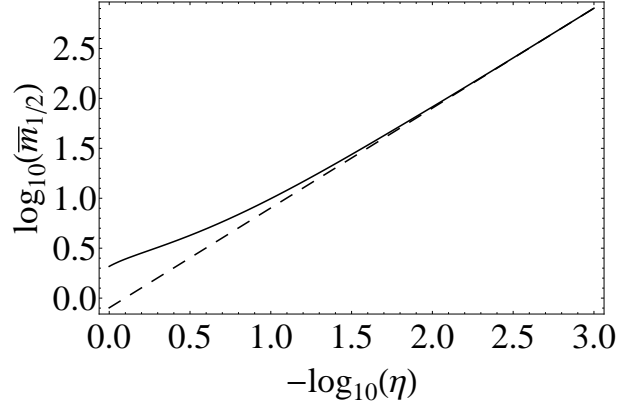


FIG. 4. Log-log plot of the characteristic average photon number of the EPR state needed to obtain entanglement, $\bar{m}_{1/2}$, vs the effective detector efficiency, η , showing the range of validity for scaling. The dashed line corresponds to the asymptotic scaling law of $\bar{m}_{1/2} = 0.80/\eta$.

tive measurements, while the probability for false positive measurements may be significant due to the inability to discern the parity of the photon number with low efficiency detectors. The probability to obtain false positive results equals the total positive measurement probability, the probability for at least one click at each detector, minus the true positive probability. It is found in analogy with the derivation leading to Eq. (31) and is

$$\text{ProbFP}(\bar{m}, \eta) = \sum_{n_1=1}^{\infty} \sum_{n_2=1}^{\infty} \overline{\text{Prob}}_{n_1, n_2}(\bar{m}) \times [1 - (1 - \eta)^{n_1}][1 - (1 - \eta)^{n_2}] - \text{ProbSucc}(\bar{m}, \eta). \quad (36)$$

By noting that $\overline{\text{Prob}}_{n_1, n_2}$ varies relatively smoothly as a function of its arguments, one finds the false positive probability to be of the same order of magnitude as the true positive probability.

There are many ways to cope with false positive measurements. One method is entanglement distillation through local operations and classical communications (LOCC) of all the positive measurement QD pairs obtained.⁶⁷ Other methods include performing a Bell measurement on the two QDs or unambiguous state discrimination via the projectors: $\hat{\pi}_1 = |\Psi_{-}\rangle\langle\Psi_{-}|$, $\hat{\pi}_2 = 1 - |\Psi_{-}\rangle\langle\Psi_{-}|$. This projective measurement enables us to pick out all the Bell state pairs without affecting their states.¹

Currently, the two aforementioned methods are not available for QD spin qubits, and hence we suggest avoiding the false positive readings problem by using low-noise high-efficiency photon-number-resolving detectors. In recent years, such detectors with efficiencies in the range of 90-95% were developed.⁶⁸⁻⁷⁰ If we use detectors of high efficiency in our scheme and can keep the optical transmission factors high, leading to an effective detector efficiency above 80%, then using $\bar{m} = 5$ will enable us to

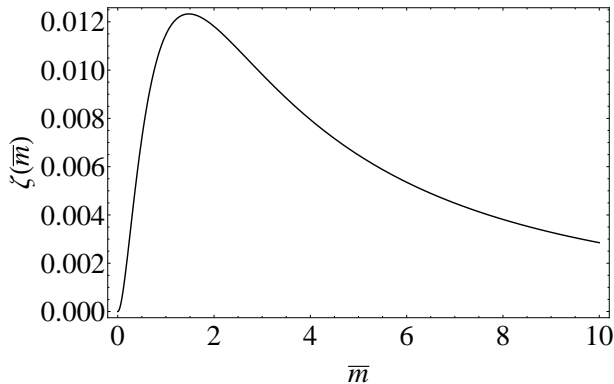


FIG. 5. Plot of $\zeta(\bar{m})$, the coefficient of the first order correction in $(1 - \eta)$ to the success probability of an ideal detector, vs \bar{m} , the average photon number at the input EPR state. The effective detector efficiency, η , is assumed to be close to 1. The maximum occurs for $\bar{m} = 1.47$ and is 0.0123.

discern between even and odd number of photons, largely eliminate the false positive counts and obtain close to asymptotic performance. In comparison, the low entanglement generation rate in single-photon schemes entails a higher ratio of false positive to true positive measurements due to detector dark counts, and this, in turn, translates to a lower entanglement fidelity.^{32,71}

We now wish to show that our scheme outperforms single-photon schemes also in this near-ideal detector regime. Even though the success probability for some single-photon schemes^{32,72} is $\eta^2/4$, which leads to an asymptotic $\eta = 1$ limit of $1/4$, compared with $1/16$ in our scheme, the single-photon schemes suffer from a factor of the order of 0.1 in η , which currently cannot be eliminated, due to nonideal single-photon sources. Moreover, the multiphoton state is more robust against noise, due to the fluorescence signal being redundantly encoded in multiple components of the state as can be qualitatively seen from Eq. (8). This claim is quantitatively confirmed by writing the success probability as a series in the small parameter $(1 - \eta)$,

$$\text{ProbSucc}(\bar{m}, \eta) = \text{ProbSucc}(\bar{m}, 1) - \zeta(\bar{m})(1 - \eta) + O((1 - \eta)^2). \quad (37)$$

While for the single-photon schemes, $\zeta(\bar{m}) = 1/8$, for our scheme $\zeta(\bar{m})$, found numerically from Eq. (31), is plotted in Fig. 5 and is bound from above by 0.0123 which is more than 10 times lower than the single-photon result. For $\bar{m} = 5$ suggested above this ratio is even greater.

VI. CONCLUSIONS

In this work, we demonstrated a simple, effective and robust protocol for generating entanglement between two stationary QD spin qubits using multiphoton Gaussian

states. Our method is clearly distinguished from current single-photon schemes by the absence of fragile single-photon states and noisy vacuum states and by unitary evolution before measurement in a spin qubit 4-level system, rather than spontaneous emission in a 3-level one. We showed resonance fluorescence entails entanglement between the photon and qubit states, and that measurement of photon numbers can herald a maximally entangled state of the QDs. The association of this state with two odd measurements was observed to be a consequence of the bosonic nature of photons via the *multiphoton Hong-Ou-Mandel effect*. For nonideal optical elements and photon number detectors, we pointed that, owing to the robustness to noise of the Gaussian states, the same success probability as in the ideal case can be obtained by an increase of the number of photons at the input. We then proposed the recently developed near-ideal detectors as means for decreasing false positive readings at the photon detectors, and found that also in this regime Gaussian states make our system less prone to noise than parallel single-photon schemes.

Throughout the paper we assumed the two QDs are identical, as are the two input EPR states, whereas, in practice, the parameter values may differ. We now show the results are maintained if the discrepancy is not too large. First, a resonance frequency difference between the QDs does not change the results if it is much lower than the trion state linewidth. Second, if the input EPR states parameters are λ and $\lambda + \Delta\lambda$, and the QD coupling constants are g and $g + \Delta g$, then with $\bar{m} > 2$, $\Delta\lambda/\lambda < 0.01\%$ and $\Delta g/g < 0.01\%$, the expected fidelity of the qubit state relative to $|\Psi^-\rangle$ upon two odd photon number measurements at $0 < t < 40\pi/g$ is found to be higher than 99.7%.

With the caveats given following Eq. (3) concerning the system presented here not being a fully fledged experimental design, we hereby estimate the entanglement creation rate. The ideal photon process is now assumed to take place with QDs in microcavities and thus exhibits losses, which are now estimated. The strong coupling regime, which was experimentally realized in microcavities,^{73,74} is defined by $\Gamma_{cav}/2 < \Omega$,⁷⁵ where $\Gamma_{cav} = \omega/Q$ is the cavity decay rate, ω is the radiation frequency, Q is the cavity quality factor, and Ω is the Rabi frequency. In this regime, assumed here, Rabi oscillations have a decay rate Γ_{cav} . The present collection efficiency of light out of a planar microcavity containing a QD can be made to be better than 10%.^{19,20,73} The probability for resonance fluorescence in the microcavity, in turn, can be made to be higher than 50%.⁷³ By taking these lower limits, the probability for resonance fluorescence and successful collection from each quantum dot is $C \approx 5\%$. QD spin qubit state initialization in the Faraday geometry was performed within $\sim 1 \mu\text{s}$,⁵⁷ while EPR states were prepared in $\sim 1.3 \mu\text{s}$.^{62,63} With photodetection time being much shorter,¹⁹ the repetition rate R is approximately the reciprocal of the larger of these two times. If we now assume that the aver-

age number of photons in the Gaussian states is large enough for the success probability to reach its characteristic value of $P = 1/32$, the entanglement generation rate is $C^2PR \approx 3.6 \cdot 10^3 \text{ min}^{-1}$, which is 3 orders of magnitude larger than the single-photon heralded entanglement creation rate.^{28,29,32–34} In addition, the spin qubit entanglement fidelity may be expected to be close to unity assuming high-fidelity preparations of the QD states and Gaussian photon states.

The experimental realization of this proposed entanglement method may be an important step towards fast and scalable quantum computation and communication. More generally, our work provides one illustration of Gaussian photon states being a viable alternative to single-photon ones as information carriers. In analogy, future work may be the application of spin Gaussian states to replace single-spin qubits as information carriers. Another direction may be to explore the use of spin qubits to influence photon Gaussian states for Gaussian information processing. Our method also has a limitation. The selection rules in the Faraday geometry provide excellent insulation of two-photon state evolution paths, which can be utilized for distant entanglement of stationary qubits. The Voigt geometry has many advantages, such as fast initial state preparation,⁷⁶ but our entanglement method will have to be drastically redesigned in this geometry, as its selection rules allow transitions between each spin state and both trion states.

Appendix A: Gaussian States

We provide the detail for writing down the input Gaussian state with conditions specified in Sec. II. A Gaussian state can be defined via its Wigner quasiprobability distribution, given by³⁸

$$W(\mathbf{x}) = \frac{\exp[-(1/2)(\mathbf{x} - \bar{\mathbf{x}})^T \mathbf{V}^{-1}(\mathbf{x} - \bar{\mathbf{x}})]}{(2\pi)^N \sqrt{\det \mathbf{V}}}, \quad (\text{A1})$$

where

$$\mathbf{x} = (q_1, p_1, q_2, p_2, \dots, q_N, p_N), \quad (\text{A2})$$

$$\bar{\mathbf{x}} = (\bar{q}_1, \bar{p}_1, \bar{q}_2, \bar{p}_2, \dots, \bar{q}_N, \bar{p}_N), \quad (\text{A3})$$

$$V_{ij} = \frac{1}{2} \langle \hat{x}_i \hat{x}_j + \hat{x}_j \hat{x}_i \rangle - \langle \hat{x}_i \rangle \langle \hat{x}_j \rangle, \quad (\text{A4})$$

are the phase space coordinates vector, displacement vector and covariance matrix, respectively, with N being the number of modes. The phase space operators are given by $\hat{q}_k = (a_k + a_k^\dagger)/\sqrt{2}$ and $\hat{p}_k = -i(a_k - a_k^\dagger)/\sqrt{2}$, where \hbar is put to unity for brevity.

The Gaussian state is characterized completely by its displacement vector $\bar{\mathbf{x}}$ and covariance matrix \mathbf{V} . A general two-mode Gaussian state can be reduced by local unitary operations on each mode, which do not affect the purity and entanglement in the state, to the stan-

dard form,⁵⁰ where $\mathbf{x} = 0$ and

$$\mathbf{V} = \begin{pmatrix} s_- & 0 & h_- & 0 \\ 0 & s_- & 0 & h_+ \\ h_- & 0 & s_+ & 0 \\ 0 & h_+ & 0 & s_+ \end{pmatrix}. \quad (\text{A5})$$

Condition (3) of the same parametric strength of the two polarization modes in Sec. II is satisfied by $s_- = s_+ = s$. Condition (4) of pure state is satisfied by⁵³

$$\det(\mathbf{V}) = \frac{1}{16}. \quad (\text{A6})$$

The resulting equation

$$(s^2 - h_-^2)(s^2 - h_+^2) = \frac{1}{16} \quad (\text{A7})$$

together with $V > 0$ entails $s > \max(1/2, |h_-|, |h_+|)$.

Combining this result with the uncertainty principle for Gaussian states,⁷⁷ $V + \frac{i}{2}\Omega \geq 0$, where Ω is the usual symplectic form

$$\Omega \equiv \begin{pmatrix} 0 & 1 & 0 & 0 \\ -1 & 0 & 0 & 0 \\ 0 & 0 & 0 & 1 \\ 0 & 0 & -1 & 0 \end{pmatrix}, \quad (\text{A8})$$

gives $h_- = -h_+$, which, combined with Eq. (A7) and substituted in Eq. (A5), reduces the covariance matrix to the form

$$\mathbf{V} = \frac{1}{2} \begin{pmatrix} \nu & 0 & \sqrt{\nu^2 - 1} & 0 \\ 0 & \nu & 0 & -\sqrt{\nu^2 - 1} \\ \sqrt{\nu^2 - 1} & 0 & \nu & 0 \\ 0 & -\sqrt{\nu^2 - 1} & 0 & \nu \end{pmatrix}. \quad (\text{A9})$$

If one defines $\nu = \cosh(2r)$, then this Gaussian state describes the two-mode squeezed vacuum state,³⁸ also known as an Einstein-Podolski-Rosen (EPR) state, with the squeezing parameter $r > 0$. In the number state basis the EPR state is given by Eq. (1).

Appendix B: QD density matrix properties for even-even measurement

We show that the QD density matrix for an even-even measurement in Eq. (19) satisfies $q_\dagger \geq q_+$. Eq. (19) is obtained by tracing out the photons in $|\psi_{n_1, n_2}\rangle\langle\psi_{n_1, n_2}|$, where $|\psi_{n_1, n_2}\rangle$ is given in Eq. (18). The coefficient q_\dagger is

$$q_\dagger = \frac{1 - \lambda^2}{2} \left| P_{n_1, n_2} U_{BS} \sum_{m, m'=0}^{\infty} \lambda^{m+m'} \times \sin(g\sqrt{m}t) \sin(g\sqrt{m'}t) |m-1, m; m'-1, m'\rangle \right|^2, \quad (\text{B1})$$

and q_+ is seen to have the same form except for $|m-1, m; m'-1, m'\rangle \rightarrow |m-1, m; m', m'-1\rangle$. Up to normalization, Eq. (B1) is the probability for the state following

P_{n_1, n_2} inside the norm to be in the space projected by P_{n_1, n_2} . The norm of this state and the one of the corresponding state in q_+ are equal by the unitarity of U_{BS} .

Using the beam splitter transformation (12), we have

$$q_{\uparrow} = \frac{1-\lambda^2}{2\sqrt{2}} \left| P_{n_1, n_2} (c_+^\dagger + d_+^\dagger) U_{BS} \sum_{m, m'=0}^{\infty} \frac{1}{m'} \lambda^{m+m'} \times \sin(g\sqrt{m}t) \sin(g\sqrt{m'}t) |m-1, m, m'-1, m'-1\rangle \right|^2, \quad (\text{B2})$$

where q_+ is given by the same expression with $c_+ \rightarrow c_-$ and $d_+ \rightarrow d_-$. Consider the state appearing after $(c_+^\dagger + d_+^\dagger)$ in Eq. (B2). This state exists in both the expressions for q_{\uparrow} and q_+ . Had the operator $(c_{\pm}^\dagger + d_{\pm}^\dagger)$ not existed, Eq. (B2) would, by virtue of the total photon number, have given a nonzero result only for even-odd or odd-even (n_1, n_2) pairs. Since the state norm is iden-

tical in q_{\uparrow} and q_+ both before and after the operation of $(c_{\pm}^\dagger + d_{\pm}^\dagger)$, which adds a single photon, this operator merely shifts probability of projection from even-odd and odd-even pairs to even-even and odd-odd ones. Since q_{\uparrow} is zero for odd-odd pairs, a given even-even pair in it, (n_1, n_2) , receives all contributions from $(n_1 - 1, n_2)$ and $(n_1, n_2 - 1)$, while in q_+ it shares these contributions with the odd-odd pairs $(n_1 - 1, n_2 + 1)$ and $(n_1 + 1, n_2 - 1)$. We thus conclude that for the even-even case $q_{\uparrow} \geq q_+$.

Appendix C: Time-averaged measurement probability

We set to find the form of C_{n_1, n_2} , the time average of $g_{n_1, n_2}(t)$ in Eq. (24), which is the time-dependent part of the measurement probability. As the beam splitter conserves photon number in each polarization, Eq. (24) reduces to

$$g_{n_1, n_2}(t) = \frac{1}{2} \sum_{k=\max(n_1-n_3, 0)}^{\min(n_1, n_3)} \left[\sum_{m=1}^{n_3} A_{km} \sin(g\sqrt{m}t) \sin(g\sqrt{n_3-m+1}t) \right]^2, \quad (\text{C1})$$

$$A_{km} \equiv \langle k, n_1 - k; n_3 - k, n_3 - n_1 + k | U_{BS} | m - 1, m; n_3 - m + 1, n_3 - m \rangle. \quad (\text{C2})$$

The beam splitter matrix element can be broken to a product of two one-mode beam splitter matrix elements as

$$\langle m'_-, m'_+; \tilde{m}'_-, \tilde{m}'_+ | U_{BS} | m_-, m_+; \tilde{m}_-, \tilde{m}_+ \rangle = \langle m'_-, \tilde{m}'_- | U_{BS,1} | m_-, \tilde{m}_- \rangle \langle m'_+, \tilde{m}'_+ | U_{BS,1} | m_+, \tilde{m}_+ \rangle, \quad (\text{C3})$$

with $U_{BS,1}$ being the one-mode beam splitter operator. By Eq. (12) the matrix elements of this operator are

$$\langle k, n - k | U_{BS,1} | l, n - l \rangle = \sqrt{\frac{k!(n-k)!}{l!(n-l)!}} 2^{-n/2} \sum_{q=0}^k \binom{l}{q} \binom{n-l}{k-q} (-1)^{l+q}. \quad (\text{C4})$$

The time average of a four sines product in the expansion of Eq. (C1) is nonzero only if the four frequencies of the sines contain two identical frequency pairs. Consequently, this time average reads

$$C_{n_1, n_2} = \frac{1}{8} \sum_{m=1}^{n_3} (B_{mm} + B_{m, n_3-m+1}) - \frac{1}{32} B_{(n_3+1)/2, (n_3+1)/2} (1 - (-1)^{n_3}), \quad (\text{C5})$$

where

$$B_{mm'} \equiv \sum_{k=\max(n_1-n_3, 0)}^{\min(n_1, n_3)} A_{km} A_{km'}, \quad (\text{C6})$$

the dependence of A_{km} and $B_{mm'}$ on (n_1, n_2) being understood.

Appendix D: Success probability for nonideal detectors

We wish to find the infinite sum for the success probability with nonideal detectors in Eq. (31). Due to the additional η -dependent factor in Eq. (31), the sum rule of Eq. (28) cannot be used to remove the sum over n_1 and put it in closed form as in the ideal detectors case. Approximating Eq. (31) by summing a finite number of terms is also unsatisfactory due to the delicate convergence of this series. Equation (25) indicates that the \bar{m} -dependent part of high n_3 summands decays to zero very slowly relative to lower n_3 terms and cannot be neglected when \bar{m} is large, while C_{n_1, n_2} for these summands also does not decay with increasing n_3 , being always of the order of 1 as seen from Eq. (28). In order to find an effective approximation for the infinite sum in Eq. (31), we first need to study the properties of C_{n_1, n_2} . We use Eq. (C5) to plot the normalized C_{n_1, n_2} in Fig. 6, and observe that the normalized coefficients exhibit the property of *data collapse* when n_3 is large. In particular, we find the standard deviation of the $C_{n_1, n_2}/D_{n_3}$ distribution for a given n_3 is a linear function of n_3 .

With the properties of the C_{n_1, n_2} coefficients in mind, we set to find an approximation which will allow us to sum Eq. (31). Such an approximation, inspired by Fig. 6, is the “rooftop” approximation, wherein $C_{n_1, 2n_3-n_1}$ for a

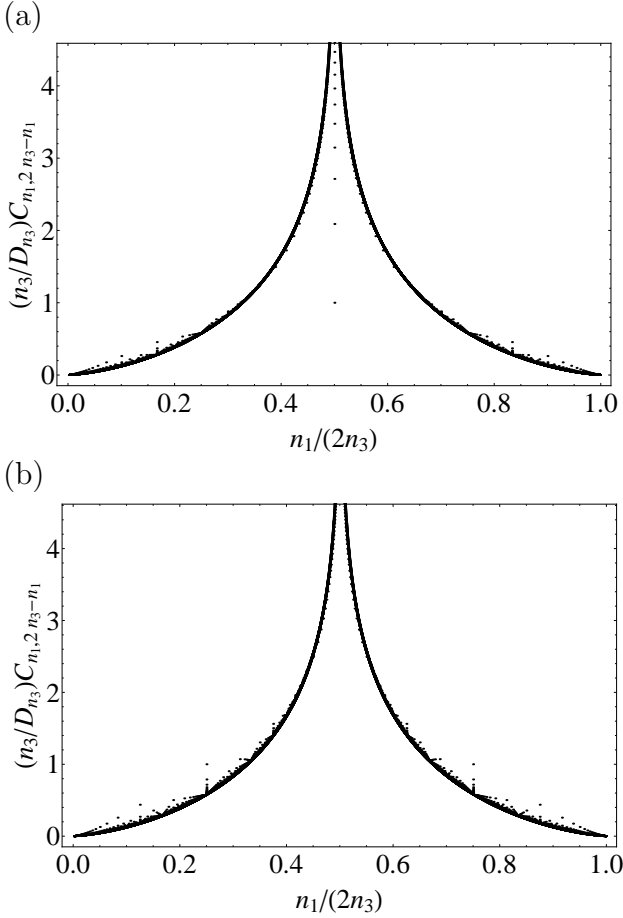


FIG. 6. Normalized values of C_{n_1, n_2} , the time average of the time-dependent part in the measurement probability, for odd (a) and even (b) values of $1 \leq n_3 \leq 300$, where $n_3 = (n_1 + n_2)/2$, and n_1 and n_2 are the photon numbers measured in the first and second detectors, respectively. The coefficient D_{n_3} is obtained by summing C_{n_1, n_2} over all pairs of odd n_1 and n_2 corresponding to a given n_3 . The normalized values of C_{n_1, n_2} exhibit the property of *data collapse* when n_3 is large.

given n_3 is a piecewise linear function of the form

$$C_{n_1, 2n_3-n_1} \approx \begin{cases} a_{n_3}n_1 + b_{n_3} & 0 \leq n_1 \leq n_3 \\ a_{n_3}(2n_3 - n_1) + b_{n_3} & n_3 \leq n_1 \leq 2n_3 \end{cases}, \quad (\text{D1})$$

where a_{n_3} and b_{n_3} are determined by two constraints: Eq. (28) and the linear relation for the standard deviation of the $C_{n_1, n_2}/D_{n_3}$ distribution. Equation (D1) is substituted in Eq. (31), which can then be exactly summed. By comparing the approximate C_{n_1, n_2} with their exact values, we find the rooftop approximation error is lower than 2%. We note the approximation is exact when $\overline{m} \rightarrow \infty$, as then the dominant terms in Eq. (31) have high n_3 and an essentially flat η -dependent factor, a fact which, combined with C_{n_1, n_2} still satisfying Eq. (28), leads to an exact result.

This insight leads to an improved approximation, the “hybrid” approximation, obtained by summing Eq. (31) up to some high value of n_3 , $n_{3, \max}$, exactly and then writing the rest of the sum in closed form using the rooftop approximation in Eq. (D1). With $n_{3, \max} = 300$, we find, by the method noted above, that the hybrid approximation error is below 1%. We use this approximation to plot Fig. 3.

ACKNOWLEDGMENTS

This research was supported by U.S. Army Research Office MURI Award No. W911NF0910406, by NSF Grant No. PHY-1104446 and by ARO (IARPA, W911NF-08-1-0487). The authors thank D. G. Steel for useful discussions.

REFERENCES

-
- * gcohen@physics.ucsd.edu
 - ¹ S. M. Barnett, *Quantum Information*, 1st ed. (Oxford University Press, New York, 2009).
 - ² G. Jaeger, *Quantum Information*, 1st ed. (Springer, New York, 2007).
 - ³ C. H. Bennett, G. Brassard, C. Crépeau, R. Jozsa, A. Peres, and W. K. Wootters, Phys. Rev. Lett. **70**, 1895 (1993).
 - ⁴ C. H. Bennett and S. J. Wiesner, Phys. Rev. Lett. **69**, 2881 (1992).
 - ⁵ H. J. Kimble, Nature (London) **453**, 1023 (2008).
 - ⁶ L. Luo, D. Hayes, T. A. Manning, D. N. Matsukevich, P. Maunz, S. Olmschenk, J. D. Sterk, and C. Monroe, Fortschr. Phys. **57**, 1133 (2009).
 - ⁷ A. Badolato, K. Hennessy, M. Atatüre, J. Dreiser, E. Hu, P. M. Petroff, and A. Imamoglu, Science **308**, 1158 (2005).
 - ⁸ P. Gallo, M. Felici, B. Dwir, K. A. Atlasov, K. F. Karlsson, A. Rudra, A. Mohan, G. Biasiol, L. Sorba, and E. Kapon, Appl. Phys. Lett. **92**, 263101 (2008).
 - ⁹ M. Pelton, C. Santori, J. Vučković, B. Zhang, G. S. Solomon, J. Plant, and Y. Yamamoto, Phys. Rev. Lett. **89**, 233602 (2002).
 - ¹⁰ E. Moreau, I. Robert, L. Manin, V. Thierry-Mieg, J. M. Gérard, and I. Abram, Physica E **13**, 418 (2002).
 - ¹¹ D. Press, T. D. Ladd, B. Zhang, and Y. Yamamoto, Nature (London) **456**, 218 (2008).
 - ¹² S. Foletti, H. Bluhm, D. Mahalu, V. Umansky, and A. Yacoby, Nat. Photonics **5**, 903 (2009).
 - ¹³ A. Greilich, S. E. Economou, S. Spatzek, D. R. Yakovlev, D. Reuter, A. D. Wieck, T. L. Reinecke, and M. Bayer, Nat. Phys. **5**, 262 (2009).
 - ¹⁴ E. D. Kim, K. Truex, X. Xu, B. Sun, D. G. Steel, A. S.

- Bracker, D. Gammon, and L. J. Sham, Phys. Rev. Lett. **104**, 167401 (2010).
- ¹⁵ R. Brunner, Y.-S. Shin, T. Obata, M. Pioro-Ladrière, T. Kubo, K. Yoshida, T. Taniyama, Y. Tokura, and S. Tarucha, Phys. Rev. Lett. **107**, 146801 (2011).
 - ¹⁶ D. Kim, S. G. Carter, A. Grelich, A. S. Bracker, and D. Gammon, Nat. Phys. **7**, 223 (2011).
 - ¹⁷ L.-B. Chen, L. J. Sham, and E. Waks, Phys. Rev. B **85**, 115319 (2012).
 - ¹⁸ M. D. Shulman, O. E. Dial, S. P. Harvey, H. Bluhm, V. Umansky, and A. Yacoby, Science **336**, 202 (2012).
 - ¹⁹ K. De Greve, L. Yu, P. L. McMahon, J. S. Pelc, C. M. Natarajan, N. Y. Kim, E. Abe, S. Maier, C. Schneider, M. Kamp, S. Höfling, R. H. Hadfield, A. Forchel, M. M. Fejer, and Y. Yamamoto, Nature (London) **491**, 421 (2012).
 - ²⁰ W. B. Gao, P. Fallahi, E. Togan, J. Miguel-Sanchez, and A. Imamoglu, Nature (London) **491**, 426 (2012).
 - ²¹ J. R. Schaibley, A. P. Burgers, G. A. McCracken, L.-M. Duan, P. R. Berman, D. G. Steel, A. S. Bracker, D. Gammon, and L. J. Sham, Phys. Rev. Lett. **110**, 167401 (2013).
 - ²² G. Bowen, Phys. Rev. A **66**, 052313 (2002).
 - ²³ L.-M. Duan, M. D. Lukin, J. I. Cirac, and P. Zoller, Nature (London) **414**, 413 (2001).
 - ²⁴ T. Brun, I. Devetak, and M.-H. Hsieh, Science **314**, 436 (2006).
 - ²⁵ S. Zippilli, G. A. Olivares-Rentería, G. Morigi, C. Schuck, F. Rohde, and J. Eschner, New Jour. Phys. **10**, 103003 (2008).
 - ²⁶ C. Cabrillo, J. I. Cirac, P. García-Fernández, and P. Zoller, Phys. Rev. A **59**(2), 1025 (1999).
 - ²⁷ L. I. Childress, J. M. Taylor, A. Sørensen, and M. D. Lukin, Phys. Rev. A **72**, 052330 (2005).
 - ²⁸ D. N. Matsukevich, P. Maunz, D. L. Moehring, S. Olmschenk, and C. Monroe, Phys. Rev. Lett. **100**, 150404 (2008).
 - ²⁹ L. Slodička, G. Hétet, N. Röck, P. Schindler, M. Hennrich, and R. Blatt, Phys. Rev. Lett. **110**, 083603 (2013).
 - ³⁰ C. Simon and W. T. M. Irvine, Phys. Rev. Lett. **91**, 110405 (2003).
 - ³¹ L.-M. Duan and H. J. Kimble, Phys. Rev. Lett. **90**, 253601 (2003).
 - ³² D. L. Moehring, P. Maunz, S. Olmschenk, K. C. Younge, D. N. Matsukevich, L.-M. Duan, and C. Monroe, Nature (London) **449**, 68 (2007).
 - ³³ P. Maunz, S. Olmschenk, D. Hayes, D. N. Matsukevich, L.-M. Duan, and C. Monroe, Phys. Rev. Lett. **102**, 250502 (2009).
 - ³⁴ J. Hofmann, M. Krug, N. Ortegel, L. Gérard, M. Weber, W. Rosenfeld, and H. Weinfurter, Science **337**, 72 (2012).
 - ³⁵ P. van Loock, T. D. Ladd, K. Sanaka, F. Yamaguchi, K. Nemoto, W. J. Munro, and Y. Yamamoto, Phys. Rev. Lett. **96**, 240501 (2006).
 - ³⁶ Y. P. Huang and M. G. Moore, Phys. Rev. A **77**, 032349 (2008).
 - ³⁷ C.-K. Chan and L. J. Sham, Phys. Rev. Lett. **110**, 070501 (2013).
 - ³⁸ C. Weedbrook, S. Pirandola, R. García-Patrón, N. J. Cerf, T. C. Ralph, J. H. Shapiro, and S. Lloyd, Rev. Mod. Phys. **84**, 621 (2012).
 - ³⁹ S. L. Braunstein and P. van Loock, Rev. Mod. Phys. **77**, 513 (2005).
 - ⁴⁰ F. Grosshans and P. Grangier, Phys. Rev. Lett. **88**, 057902 (2002).
 - ⁴¹ S. L. Braunstein and H. J. Kimble, Phys. Rev. Lett. **80**, 869 (1998).
 - ⁴² A. S. Holevo and R. F. Werner, Phys. Rev. A **63**, 032312 (2001).
 - ⁴³ M. Gu, C. Weedbrook, N. C. Menicucci, T. C. Ralph, and P. van Loock, Phys. Rev. A **79**, 062318 (2009).
 - ⁴⁴ N. J. Cerf and S. Iblisdir, Phys. Rev. A **62**, 040301 (2000).
 - ⁴⁵ T. C. Ralph and E. H. Huntington, Phys. Rev. A **66**, 042321 (2002).
 - ⁴⁶ J. Jing, J. Zhang, Y. Yan, F. Zhao, C. Xie, and K. Peng, Phys. Rev. Lett. **90**, 167903 (2003).
 - ⁴⁷ H. Takahashi, J. S. Neergaard-Nielsen, M. Takeuchi, M. Takeoka, K. Hayasaka, A. Furusawa, and M. Sasaki, Nat. Photonics **4**, 178 (2010).
 - ⁴⁸ V. D'Auria, S. Fornaro, A. Porzio, S. Solimeno, S. Olivares, and M. G. A. Paris, Phys. Rev. Lett. **102**, 020502 (2009).
 - ⁴⁹ D. Buono, G. Nocerino, V. D'Auria, A. Porzio, S. Olivares, and M. G. A. Paris, J. Opt. Soc. Am. B **27**, A110 (2010).
 - ⁵⁰ L.-M. Duan, G. Giedke, J. I. Cirac, and P. Zoller, Phys. Rev. Lett. **84**, 2722 (2000).
 - ⁵¹ G. Giedke, M. M. Wolf, O. Krüger, R. F. Werner, and J. I. Cirac, Phys. Rev. Lett. **91**, 107901 (2003).
 - ⁵² G. Vidal and R. F. Werner, Phys. Rev. A **65**, 032314 (2002).
 - ⁵³ A. Serafini, F. Illuminati, and S. De Siena, J. Phys. B: At. Mol. Opt. Phys. **37**, L21 (2004).
 - ⁵⁴ P. Giorda and M. G. A. Paris, Phys. Rev. Lett. **105**, 020503 (2010).
 - ⁵⁵ D. Kim, S. E. Economou, S. C. Bădescu, M. Scheibner, A. S. Bracker, M. Bashkansky, T. L. Reinecke, and D. Gammon, Phys. Rev. Lett. **101**, 236804 (2008).
 - ⁵⁶ X. Xu, B. Sun, P. R. Berman, D. G. Steel, A. S. Bracker, D. Gammon, and L. J. Sham, Nat. Phys. **4**, 692 (2008).
 - ⁵⁷ M. Atatüre, J. Dreiser, A. Badolato, A. Högele, K. Karrai, and A. Imamoglu, Science **312**, 551 (2006).
 - ⁵⁸ E. T. Jaynes and F. W. Cummings, Proc. IEEE **51**, 89 (1963).
 - ⁵⁹ W. K. Wootters, Phys. Rev. Lett. **80**, 2245 (1998).
 - ⁶⁰ C. K. Hong, Z. Y. Ou, and L. Mandel, Phys. Rev. Lett. **59**, 2044 (1987).
 - ⁶¹ P. R. Berman and V. S. Malinovsky, *Principles of Laser Spectroscopy and Quantum Optics*, 1st ed. (Princeton University Press, Princeton, 2011).
 - ⁶² J. Wenger, A. Ourjoumtsev, R. Tualle-Brouiri, and P. Grangier, Eur. Phys. J. D **32**, 391 (2005).
 - ⁶³ A. Ourjoumtsev, R. Tualle-Brouiri, and P. Grangier, Phys. Rev. Lett. **96**, 213601 (2006).
 - ⁶⁴ X. Xu, W. Yao, B. Sun, D. G. Steel, A. S. Bracker, D. Gammon, and L. J. Sham, Nat. Lett. **459**, 1105 (2009).
 - ⁶⁵ D. Press, K. De Greve, P. L. McMahon, T. D. Ladd, B. Friess, C. Schneider, M. Kamp, S. Höfling, A. Forchel, and Y. Yamamoto, Nat. Photonics Lett. **4**, 367 (2010).
 - ⁶⁶ P. M. Chaikin and T. C. Lubensky, *Principles of Condensed Matter Physics*, 1st ed. (Cambridge University Press, Cambridge, 1995).
 - ⁶⁷ C. H. Bennett, H. J. Bernstein, S. Popescu, and B. Schumacher, Phys. Rev. A **53**, 2046 (1996).
 - ⁶⁸ D. Rosenberg, A. E. Lita, A. J. Miller, and S. W. Nam, Phys. Rev. A **71**, 061803(R) (2005).
 - ⁶⁹ G. Khoury, H. S. Eisenberg, E. J. S. Fonseca, and D. Bouwmeester, Phys. Rev. Lett. **96**, 203601 (2006).
 - ⁷⁰ A. E. Lita, A. J. Miller, and S. W. Nam, Opt. Express **16**, 3032 (2008).
 - ⁷¹ B. B. Blinov, D. L. Moehring, L.-M. Duan, and C. Monroe, Nat. Lett. **428**, 153 (2004).

- ⁷² S. Olmschenk, D. N. Matsukevich, P. Maunz, D. Hayes, L.-M. Duan, and C. Monroe, *Science* **323**, 486 (2009).
- ⁷³ S. Ates, S. M. Ulrich, S. Reitzenstein, A. Löffler, A. Forchel, and P. Michler, *Phys. Rev. Lett.* **103**, 167402 (2009).
- ⁷⁴ A. Löffler, J. P. Reithmaier, G. Sek, C. Hofmann, S. Reitzenstein, M. Kamp, and A. Forchel, *Appl. Phys. Lett.* **86**, 111105 (2005).
- ⁷⁵ G. Grynberg, A. Aspect, and C. Fabre, *Introduction to Quantum Optics*, 1st ed. (Cambridge University Press, Cambridge, 2010).
- ⁷⁶ X. Xu, Y. Wu, B. Sun, Q. Huang, J. Cheng, D. G. Steel, A. S. Bracker, D. Gammon, C. Emary, and L. J. Sham, *Phys. Rev. Lett.* **99**, 097401 (2007).
- ⁷⁷ R. Simon, N. Mukunda, and B. Dutta, *Phys. Rev. A* **49**, 1567 (1994).